Calorimetric study of the smectic-*A*–hexatic-*B* transition in 3(10)OBC

H. Haga and C. W. Garland
School of Science and Center for Material Science and Engineering, Massachusetts Institute of Technology, Cambridge, Massachusetts 02139
(Received 12 May 1997)

High-resolution calorimetry has been used to study the smectic-*A*(Sm-*A*)–hexatic-*B*(Hex-*B*) transition in *n*-propyl-4′-*n*-decyloxybiphenyl-4-carboxylate [3(10)OBC]. This transition is clearly first order with substantial pretransitional heat capacity wings. Power law fits to ΔC_p are possible and yield an effective ''critical'' exponent $\alpha_{\rm eff}=0.68\pm0.10$ and a discontinuity in the ''critical'' background term B_c. These results are compatible with those recently reported for the homolog 65OBC, where the first order character is very weak and subtle. The nature of the Sm-*A*–Hex-*B* transition appears to be *quasicritical*, which could be the result of a coupling between the amplitude of the bond-orientational order and in-plane positional strain.
[S1063-651X(98)03401-1]

PACS number(s): 64.70.Md, 64.60.Fr, 65.20.+w

I. INTRODUCTION

The phase transition in bulk liquid crystals between the smectic-*A* (Sm-*A*) phase, which exhibits liquidlike in-plane behavior, and the hexatic-*B* (Hex-*B*) phase, which exhibits long-range bond orientational order and significant but short-range in-plane positional order, is still a challenge after more than 15 years of experimental and theoretical work. The thermal properties of stacked hexatic phases have been reviewed by Huang and Stoebe [1], and several structural studies of the Hex-*B* and analogous tilted hexatic phases have been published [2–6]. Since the bond-orientational (BO) order parameter $\Psi=|\Psi|\exp(i6\psi)$ describing the sixfold azimuthal modulation has *XY* symmetry, it was expected that the critical Sm-*A*–Hex-*B* behavior would conform to three-dimensional (3D) *XY* universality. However, numerous experiments show ''critical'' behavior that deviates markedly from this prediction. Numerous theories have been put forward to address coupling between Ψ and various other quantities: herringbone order (orientational order that occurs in the crystal-*E* phase) [7], in-plane density and strain [8], the phase of Ψ with positional density like that occurring in the plastic crystal-*B* (Cr-*B*) phase [9], and the phase of Ψ with smectic layer fluctuations u [10]. Unfortunately, none of these theories has explained effective C_p critical exponents in the range $\alpha_{\rm eff}=0.48$ to 0.64 [1] or effective order parameter exponents $\beta_{\rm eff}=0.15$ to 0.25 [5,11,12].

Extensive experimental work on the Sm-*A*–Hex-*B* transition has been done on the homologous series *n*-alkyl-4′-*n*-alkoxybiphenyl-4-carboxylate, which has the structural formula

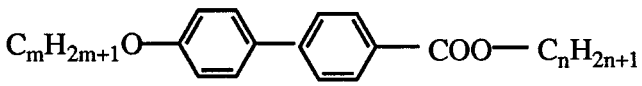

and the conventional name *nm*OBC. Most of this series exhibits the phase sequence Cr-*K*–Cr-*E*–Hex-*B*–Sm-*A*–I, where Cr-*K* is the rigid crystal form stable at room temperature, Cr-*E* is a 3D plastic crystal with herringbone orientational order (HBO), and I is the isotropic phase. It has, however, been shown that coupling to HBO has no significant effect on the Sm-*A*–Hex-*B* transition (except perhaps very close to the Sm-*A*–Hex-*B*–Cr-*E* triple point) [13]. Furthermore, systems exhibiting the Cr-*B*–Hex-*B*–Sm-*A* sequence with no indications of even short-range HBO have the same anomalous $\beta_{\rm eff}$ values for the Sm-*A*–Hex-*B* transition as Cr-*E*–Hex-*B*–Sm-*A* materials [5,12].

Sm-*A*–Hex-*B* transitions in bulk *nm*OBC compounds have been characterized as continuous second-order transitions in spite of significant rounding in the C_p peak near T_c [1,13–16]. Thermal hysteresis is also reported to be absent for these compounds within an experimental resolution of 3 mK [1,17]. However, a recent high-resolution ac calorimetric study of bulk 65OBC revealed subtle but persuasive evidence of a *very weak* first-order character for the Sm-*A*–Hex-*B* transition although the excess heat capacity ΔC_p could be well fit with a power law yielding the critical exponent 0.65 ± 0.05 [18]. The present work involves an ac calorimetric study of 3(10)OBC, another *nm*OBC compound previously reported to be second order [1,13–16]. In this case, we find unambiguous evidence of a distinct first-order character. Moreover, evidence is presented that the 3(10)OBC data in Ref. [16] are also consistent with first-order rather than second-order character. This detailed look at the fit of earlier published data was not possible for 65OBC since incomplete information was available on the fitting parameters for that compound [1]. As a result of the new calorimetric data on both 65OBC and 3(10)OBC, the previous assignment of Sm-*A*–Hex-*B* transitions in *nm*OBC as second order is called into serious question. It is hoped that these C_p studies will inspire new high-resolution Sm-*A*–Hex-*B* work with other techniques and will also stimulate new theoretical efforts.

The experimental results are described in Sec. II. A power law analysis, carried out in spite of the presence of a two-phase coexistence region associated with the weak first-order character, is presented in Sec. III, and a discussion of the Sm-*A*–Hex-*B* transition in 3(10)OBC is given in Sec. IV.

II. EXPERIMENTAL RESULTS

The compound 3(10)OBC ($M=396.5$ g mol^{-1}) exhibits the phase sequence

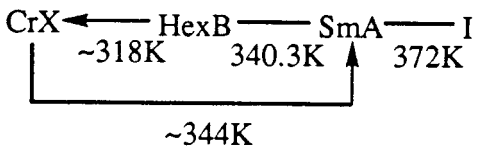

where the approximate transition temperatures are taken from Refs. [13–15]. The crystal phase Cr-*X* is of unknown structure [13] but is presumably the same as the phase Cr-*K* that is stable at room temperature. Although the Cr-*E* plastic crystal is not stable for 3(10)OBC, it is seen in 1(10)OBC, 2(10)OBC, and 2(10)OBC+3(10)OBC mixtures containing up to 86 wt. % 3(10)OBC [13]. Furthermore, Stoebe *et al.* [19] report that films of 3(10)OBC in the Hex-*B* phase show weak diffuse herringbone diffraction spots that indicate short-range HBO. It should also be noted that 4(10)OB exhibits a first-order Sm-*A*–Hex-I transition, and mixtures of 3(10)OBC+4(10)OBC with 72.6–74.3 wt. % 4(10)OBC exhibit the sequence Sm-*A*–Hex-*B*–Hex-I, where the Sm-*A*–Hex-*B* transition is probably first order [15].

Our 3(10)OBC sample, which was synthesized by J. W. Goodby and obtained from C. C. Huang, was from a different synthetic batch than that used in Refs. [13–16]. The crystalline material melted at 345.84 K when heated at a rate of +0.1 K/h, and the behavior of C_p on melting included a very sharp drop between 345.76 and 345.91 K, which is indicative of a high-purity sample. On cooling at a rate of −0.02 K/h, Sm-*A* froze at 340.08 K. This temperature is above our Sm-*A*–Hex-*B* transition temperature of ~339.6 K, making that transition monotropic. Thus faster cooling rates must be used to study it. On cooling from above 346 K at −0.2 K/h to ~336 K and then without a long delay heating at +0.2 K/h, C_p data can be obtained through the Sm-*A*–Hex-*B* transition on both heating and cooling. However, even when 3(10)OBC in the Hex-*B* phase was cooled at the rapid rate of −0.5 K/h it froze at ~330.23 K. Thus the freezing temperature is very sensitive to the cooling scan rate, and faster cooling was presumably used in Refs. [13–16].

Many runs were made on two cells containing 3(10)OBC. A small mass of liquid crystal (6.4 or 26.4 mg) was cold-weld sealed into a silver cell. Cell 1 was ~0.75 mm thick and filled with liquid crystal plus a helical coil of gold wire to enhance the internal thermal conductivity, and cell 2 was 0.5 mm thick but contained only a 0.1 mm thick layer of 3(10)OBC and an air gap. The data to be power law analyzed in Sec. III were from cooling run 2c with the latter cell, but there was good agreement among runs made on both cells. The Sm-*A*–Hex-*B* transition temperature was quite stable with time; the T_c drift for cell 1 was less than 1 mK over two weeks, and a T_c drift of +3.6 mK/d was observed for cell 2. Thus cell 2 data taken over a 1 K range near the Sm-*A*–Hex-*B* transition were subject to a T_c drift of only 1.5 mK. The high-resolution ac calorimeters have been described elsewhere [20], and the equations for processing the observed T_{ac} response to a $|P_{ac}|\exp(i\omega t)$ heat input are given in Refs. [18] and [21]. The standard frequency $\omega_0 = 0.196\ s^{-1}$ used in most previous work corresponds to a T_{ac} period of 32 s or a frequency $f=\omega_0/2\pi$ of 31.25 mHz. In the *one-phase region,* one has

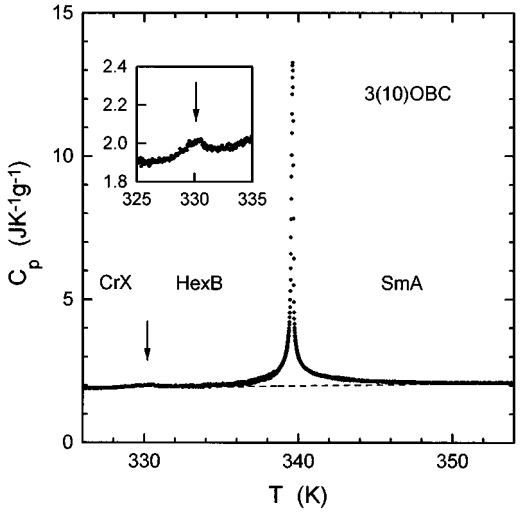

FIG. 1. Heat capacity of 3(10)OBC observed in a cooling run on cell 2 (run 2c) with an ac calorimeter operating at $\omega_0/2$ ($f=15.62$ mHz). The dashed line represents the noncritical background heat capacity. The tiny peak marked by the arrow represents the freezing of Hex-*B* on cooling at the rate −0.5 K/h below 335 K, and this region is shown in the inset on an enlarged scale.

$$C_p[C'_{\text{filled}}(\omega,T)-C_{\text{empty}}]/m, \tag{1}$$

$$C''_{\text{filled}}=0, \tag{2}$$

where C_{empty} is the heat capacity of the empty cell plus gold wire determined at ω_0 and m is the mass of 3(10)OBC in grams. C'_{filled} and C''_{filled} are the real and imaginary components of the heat capacity of a cell containing liquid crystal. Data were obtained for both cells at ω_0, $\omega_0/2$, and $\omega_0/5$ (31.25, 15.625, and 6.25 mHz).

Figure 1 shows an overview of C_p at $\omega_0/2$ over a wide temperature range for cooling run 2c, which was carried out at a scan rate of −100 mK/h near the transition temperature. Identical results were obtained for C_p as a function of $(T-T_{\text{peak}})$ over the 320–355 K temperature range for cooling runs at ω_0 and $\omega_0/5$, except that the magnitude of C_p at ω_0 is lower over the region $T_{\text{peak}}-0.125$ K to $T_{\text{peak}}+0.085$ K, where $T_{\text{peak}}=339.633$ K is the position of the maximum observed C_p value. Shown in Fig. 2 is the excess heat capacity associated with the Sm-*A*–Hex-*B* transition, obtained from

$$\Delta C_p = C_p - C_p(\text{background}), \tag{3}$$

where $C_p(\text{background})=B_r+E(T-T_c)$ represents the noncritical heat capacity that would be observed in the absence of this transition. The thermodynamic first-order transition temperature T_1 lies somewhere in the coexistence region to be discussed below. The C_p(background) term, given by the dashed line in Fig. 1, is described by $1.989+0.00068\,(T-T_c)$, where $T_c=339.61$ K was taken as the effective ''critical temperature'' (see the power law fits in Sec. III). Also shown in Fig. 2 are values of ΔC_p obtained from data in Refs. [13] and [16]. The latter data were obtained at ~1 Hz on very thin cells (thickness ~60 μm of liquid crystal), and we have assumed a 3(10)OBC density of 1.0 g cm^{-3}. The C_p(background) lines used were 2.10

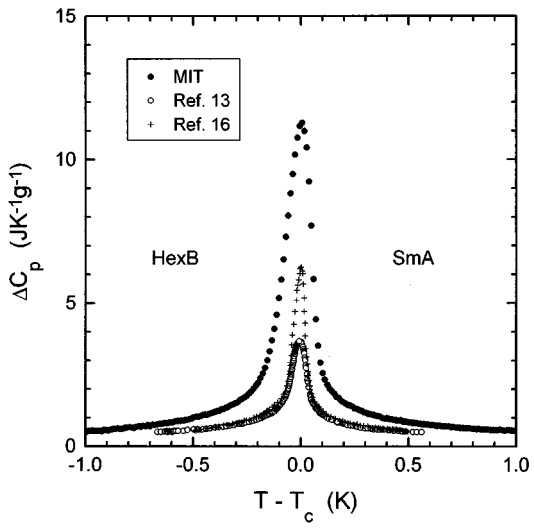

FIG. 2. Comparison of ΔC_p(Sm-A–Hex-B) data for 3(10)OBC obtained at MIT in run 2c with ΔC_p values from Refs. [13] and [16]. See text for further details.

$+0.01\Delta T$ J K^{-1} g^{-1} for data from Ref. [13] and $2.77+0.02\Delta T$ J K^{-1} g^{-1} for data from Ref. [16]; in the latter case, this is a linear version of the background curve given in Ref. [16]. It is clear from Fig. 2 that there are substantial differences in the magnitude of ΔC_p obtained in the present work and that inferred from Refs. [13] and [16]. In order to match the present ΔC_p data at $T_c \pm 0.6$ K, which is the broadest range of data available from [13] and [16], one needs to scale the previous excess heat capacities up by a factor of 1.4. This scaling factor is similar to that needed for 65OBC, where scaling ΔC_p works very well [18]. However, the overall agreement is poor for 3(10)OBC even after such scaling. Much better agreement can be achieved between the present ΔC_p and scaled excess heat capacities from Huang's group if one chooses C_p(background) values of $2.30+0.01\Delta T$ J K^{-1} g^{-1} for Ref. [13] and $2.95+0.08\Delta T$ J K^{-1} g^{-1} for Ref. [16]. The scaled quantities $2.6\Delta C_p$ (Ref. [13]) and $2.3\Delta C_p$ (Ref. [16]) then match the present ΔC_p values almost exactly except in the region from about $T_c-0.22$ K to $T_c+0.12$ K. As discussed below, this range corresponds to a two-phase coexistence region for our data. Although this scaling is excellent, the multiplicative factors 2.6 and 2.3 seem suspiciously high.

Let us now review the experimental evidence for a weak first-order character for the 3(10)OBC Sm-A–Hex-B transition. *First*, a hysteresis in $T_{\rm peak}$ of 14.6 mK was observed on a pair of heating and cooling runs carried out on cell 1 at a scan rate of ± 200 mK/h and frequency ω_0. The C_p wings from $T_{\rm peak}+0.120$ K to $T_{\rm peak}+5$ K and $T_{\rm peak}-0.215$ K to $T_{\rm peak}-5$ K coincide, but there is a systematic shift observed within a region 0.335 K wide near the peak. *Second*, there was an anomalous phase shift $\phi \equiv \Phi + \pi/2$, where Φ is the shift in the phase of $T_{\rm ac}$ with respect to that of $P_{\rm ac}$. An anomalous rapid increase in ϕ is a qualitative indication of two-phase coexistence and is seen routinely in ac calorimetry data through the nematic (N)-isotropic transition for example [20]. The phase shift ϕ anomaly for the two runs on cell 1 described above was 0.24 ± 0.01 K wide with the same hysteresis value of 14.6 mK. A comparable peak in ϕ occurred over 0.26 K for runs on cell 2. A good way to display an anomalous phase shift is to plot $[C_{\rm app} \sin\phi - (1/\omega R)]$, where $C_{\rm app} = |P_{\rm ac}|/\omega |T_{\rm ac}|$ and the thermal resistance R is the reciprocal of the thermal conductance K_b of the link between the sample cell and the bath. If there are no internal temperature gradients in the cell, which is valid for the present data, and no two-phase coexistence, $[C_{\rm app} \sin\phi - (1/\omega R)]$ should be zero. Figure 3 shows this quantity for three cooling runs on cell 2 carried out at different frequencies. This quantity is zero for runs 1c, 2c, and 3c over the range $T_{\rm peak} \pm 5$ K except for a peak 0.26 K wide for ω_0 and $\omega_0/2$ and ~ 0.4 K wide for $\omega_0/5$. The temperature and frequency dependences shown in Fig. 3 are incompatible with critical dynamics [21] but are exactly the sort of behavior expected in a region of two-phase coexistence. *Third*, ac calorimetry is not able to detect quantitatively latent heat effects, but a nonadiabatic scanning technique (linear-ramp relaxation method [21–22]) detected a total enthalpy change $DH \equiv (\delta H + \Delta H) = 6.37$ J g^{-1} for cell 1, where $\delta H = \int \Delta C_p dT$ is the integral over the pretransitional wings and ΔH is the latent heat. This total enthalpy is greater by 0.03 J g^{-1} than the integrated ΔC_p value δH for an ac cooling run done at $\omega_0/2$, and the extra enthalpy is in an approximately 200 mK wide region around T_c. The δH(ac) value almost certainly contains some smeared contributions from latent heat; thus ΔH has a minimum value of 0.03 J g^{-1} and might be as large as ~ 0.4 J g^{-1} for 3(10)OBC. *Fourth*, the analysis of the 3(10)OBC C_p data given in Ref. [16] yield large systematic deviations ΔC_p(obs) $-$ ΔC_p(fit) near T_c that indicate two-phase coexistence over ~ 100 mK for that sample as well.

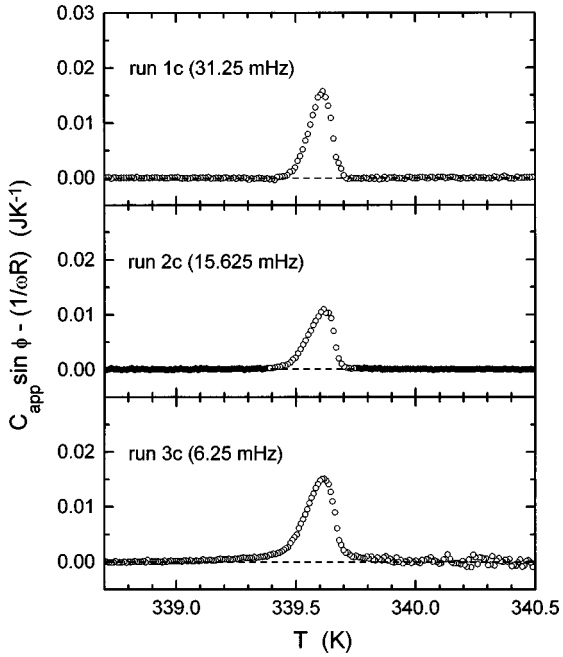

FIG. 3. Temperature dependence of $[C_{\rm app} \sin\phi - (1/\omega R)]$ near the Sm-A–Hex-B transition, where ϕ is the phase shift (see text for further details). The open circles for run 2c correspond to points whose C_p values were not used in power law fits. The anomalous (nonzero) peak indicates a region of two-phase coexistence.

III. ANALYSIS OF DATA

In spite of the weakly first-order nature of the Sm-A–Hex-B transition in 3(10)OBC, we have carried out

TABLE I. Least-squares values of the adjustable parameters for fitting ΔC_p with Eq. (4). All data except for fits 7 and 11 are from run 2c in cell 2; these two fits are to data from run 6c in cell 1. Quantities held fixed during a fit are enclosed in brackets. Range C (277 points) has $|t|_{\max} \simeq 5\times10^{-3}$, range D (565 points) has $|t|_{\max} \simeq 10^{-2}$, and range E (711 points) has $|t|_{\max} \simeq 1.5\times10^{-2}$. In all fits to run 2c, $t^{+}_{\min} \simeq 4.4\times10^{-4}$ and $t^{-}_{\min} \simeq -6.6\times10^{-4}$ in order to avoid the coexistence region. The units of $A^{\pm}$ and $B^{\pm}_c$ are J K^{-1} g^{-1}, and the estimated standard deviation σ is 0.0115 J K^{-1} g^{-1}. For all these fits, $D^{\pm}_1 \equiv 0$.

Fit	Range	T_c (K)	$\alpha^{+}_{\rm eff}$	$\alpha^{-}_{\rm eff}$	$100A^{+}$	A^{-}/A^{+}	B^{+}_c	B^{-}_c	χ^2_ν
1	C	339.549	0.734	$[\alpha^{+}_{\rm eff}]$	0.836	0.916	−0.048	$[B^{+}_c]$	4.90
2	D	339.531	0.675	$[\alpha^{+}_{\rm eff}]$	1.385	0.844	−0.122	$[B^{+}_c]$	7.34
3	E	339.527	0.664	$[\alpha^{+}_{\rm eff}]$	1.518	0.830	−0.133	$[B^{+}_c]$	7.27
4	C	339.596	0.701	$[\alpha^{+}_{\rm eff}]$	0.877	1.391	0.019	−0.209	1.09
5	D	339.598	0.683	$[\alpha^{+}_{\rm eff}]$	1.017	1.366	−0.009	−0.224	1.49
6	E	339.596	0.680	$[\alpha^{+}_{\rm eff}]$	1.063	1.330	−0.023	−0.220	1.70
7[a]	0.012	339.597	0.707	$[\alpha^{+}_{\rm eff}]$	0.861	1.347	−0.011	−0.215	1.55
8	C	339.631	0.545	0.824	2.720	0.196[b]	−0.120	$[B^{+}_c]$	0.90
9	D	339.634	0.532	0.817	3.005	0.189[b]	−0.134	$[B^{+}_c]$	1.13
10	E	339.632	0.536	0.812	2.937	0.199[b]	−0.135	$[B^{+}_c]$	1.10
11[a]	0.012	339.638	0.535	0.791	2.950	0.230[b]	−0.152	−0.169	1.11

[a]These fits are for run 6c in cell 1, where $t^{+}_{\min} = 2.9\times10^{-4}$ and $t^{-}_{\min} = -7.8\times10^{-4}$.
[b]Note that the A^{-}/A^{+} ratio does not have any universality significance since $\alpha^{+} \neq \alpha^{-}$ and $A^{\pm}$ values are strongly coupled to $\alpha^{\pm}$.

power law fits. This is feasible since the width of the two-phase coexistence region is only moderate (~0.24 K for cell 1 and ~0.26 K for cell 2) and the pretransitional wings are substantial. Such a fitting procedure will allow a comparison with published $\alpha_{\rm eff}$ critical exponents for 3(10)OBC and the $\alpha_{\rm eff}$ value recently obtained for 65OBC, where the first-order character is extremely weak.

Fits to ΔC_p data of run 2c obtained at $\omega_0/2(f = 15.6$ mHz) with cell 2 and run 6c obtained at ω_0 (31.25 mHz) with cell 1 were based on the empirical form

$$\Delta C_p^{\pm} = A^{\pm}|t|^{-\alpha_{\rm eff}}(1 + D_1^{\pm}|t|^{\Delta}) + B_c^{\pm}, \qquad (4)$$

where $t = (T - T_c)/T_c$ is the reduced temperature and $B^{\pm}_c$ is a critical contribution to the regular nonsingular behavior. A detailed discussion of the theoretical ΔC_p power law expression expected and observed for 3D XY liquid crystal systems is given in Ref. [23]. The critical C_p exponent is denoted as $\alpha_{\rm eff}$ since these Sm-A–Hex-B data are formally first order and do not yield a value for α that corresponds to any presently known second-order universality class. Usually, the correction exponent Δ is the corrections-to-scaling exponent $\Delta_1 \simeq 0.5$. Note that if $\alpha_{\rm eff} > 0.5$, the correction term $A^{\pm}D^{\pm}_1 t^{\Delta_1 - \alpha_{\rm eff}}$ will diverge at T_c rather than going to zero as it usually does. Thus, we will explore also the purely empirical choice $\Delta = 0.75$ used in the analyses of Huang's group [1,13–16]. The usual scaling constraint on B_c is $B^{+}_c = B^{-}_c$.

In order to avoid any data points in run 2c with anomalous phase shifts or C_p distortions due to two-phase coexistence, data in the range 339.380 K to 339.754 K were excluded from the fitting procedure. This means that $t^{-}_{\min} \simeq -6.56\times10^{-4}$ and $t^{+}_{\min} \simeq +4.44\times10^{-4}$. Table I shows the fitting parameters for three values of $|t|_{\max}$ with three different fitting forms. Ranges $A(|t|_{\max} = 10^{-3})$ and $B(|t|_{\max} = 3\times10^{-3})$ used for range shrinking tests of 65OBC data [18] could not be used for 3(10)OBC due to the size of the coexistence gap. Fits 1–3 are simple power-law fits with $D^{\pm}_1 = 0$ and $B^{+}_c = B^{-}_c$. These fits yield $\alpha_{\rm eff} \simeq 0.67 \pm 0.10$, where the uncertainty represents 95% confidence limits obtained with the F test. However, such fits are not very good, as indicated by the χ^2_ν values and the presence of clear systematic trends in the $\Delta C_p({\rm obs}) - \Delta C_p({\rm fit})$ residuals (not shown). Fits 4–6 allow $B^{+}_c \neq B^{-}_c$ and the quality of the fit improves significantly; see the residuals given in Fig. 4. The exponent $\alpha_{\rm eff}$ for range D and E is $\alpha_{\rm eff} = 0.68 \pm 0.10$. A comparable fit to run 6c in cell 1 is included as fit 7. Here $|t|_{\max} = 1.2\times10^{-2}$ and $\alpha_{\rm eff} = 0.71 \pm 0.10$, while the quantities

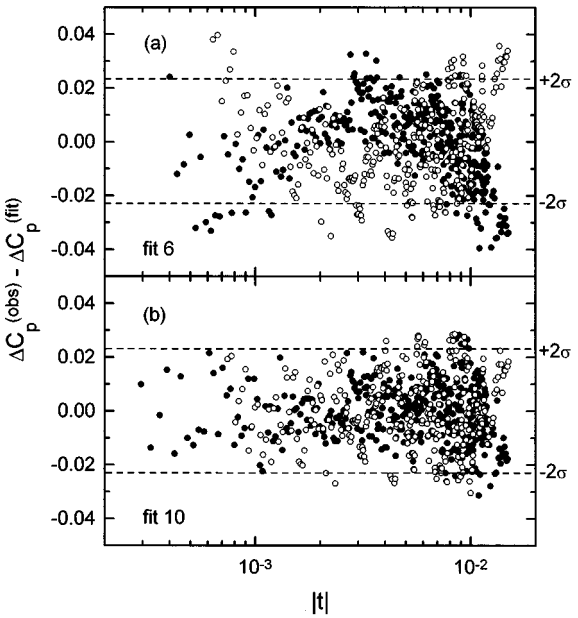

FIG. 4. Plot of residuals vs the reduced temperature t for fit 6 and fit 10 to run 2c. σ is the estimated standard deviation; ● denotes data with $T > T_c$ and ○ denotes $T < T_c$.

A^-/A^+ and $\Delta B_c = B_c^+ - B_c^-$ are both in good agreement with the results of fits 5 and 6 on run 2c in cell 2.

Fits with $B_c^+ = B_c^-$, $\Delta = 0.5$, and $D_1^\pm \neq 0$ yielded χ_ν^2 values essentially the same as fits 4–6, but the parameters for such fits are not shown since they seem physically artificial with two divergent terms ($A^\pm |t|^{-\alpha_{\rm eff}}$ and $A^\pm D_1^\pm |t|^{0.5-\alpha_{\rm eff}}$) and a D_1^-/D_1^+ ratio of 0.09–0.17 (far from the theoretically expected value of 1). The net effect of the correction term was to generate an effective step far from T_c. The value of $A^+ D_1^+ |t|^{0.5-\alpha_{\rm eff}} - A^- D_1^- |t|^{0.5-\alpha_{\rm eff}}$ is 0.208 for range D and 0.183 for range E, values that closely resemble $\Delta B_c = B_c^+ - B_c^- = 0.215$ for fit 5 and 0.197 for fit 6. Fits that allowed $T_c^+ \neq T_c^-$ did not change the $\alpha_{\rm eff}$ values or the quality of the fits since $T_c^- - T_c^+ \simeq 0.000$ to 0.002 K, which is a trivial difference. We even tried fits with a second correction term $D_2^\pm |t|$ added to Eq. (4), but such fits were completely artificial and unstable to range shrinking. Fits with Eq. (4) using Δ fixed at 0.75 and $B_c^+ = B_c^-$ gave reasonable χ_ν^2 values if the value of $\alpha_{\rm eff}$ was held fixed at Huang-like values in the 0.56–0.60 range, but the principle role of the $A^\pm D_1^\pm |t|^{0.75-\alpha_{\rm eff}}$ terms was to generate a rounded step of magnitude 0.19 at $|t| = 10^{-2}$. Furthermore, fits of this type with $\alpha_{\rm eff}$ as a free parameter yielded somewhat better fits where $\alpha_{\rm eff} = 0.86$, but the $A^\pm D_1^\pm |t|^{0.75-\alpha_{\rm eff}}$ terms dominate for $|t| > 10^{-3}$, which is unphysical.

Fits 8–11 in Table I allow scaling to be broken with $\alpha_{\rm eff}^+ \neq \alpha_{\rm eff}^-$ in view of the first-order nature of this transition. This type of fit has been employed for fitting ΔC_p at the weakly first-order N-I transition [24]. The resulting exponents yield $\alpha_{\rm eff}^- > \alpha_{\rm eff}^+$, but $\overline{\alpha_{\rm eff}} = (\alpha_{\rm eff}^+ + \alpha_{\rm eff}^-)/2$ values range from 0.66 to 0.69 in reasonable agreement with fits 4–7. Finally, a fit with $\alpha_{\rm eff}^+ \neq \alpha_{\rm eff}^-$ and $T_c^+ \neq T_c^-$ was tried since fits of that type have also been used for N-I transitions [24] and for first-order Sm-A–Hex-B transitions in n4COOBC (n-alkyl-4′-n-pentanoyloxy-biphenyl-4-carboxylates) which exhibit the Sm-A–Hex-B–Cr-B phase sequence [25]. Such fits yielded $\Delta T_c \equiv T_c^- - T_c^+$ values ranging from -0.007 to -0.013 K and $\alpha_{\rm eff}$ values very similar to fits 8–10 ($\overline{\alpha_{\rm eff}} = 0.66$).

The behavior of residuals is the best way to compare fits for possibly subtle systematic deviations, and the residuals for fits 6 and 10 from Table I are given in Fig. 4. Log-log plots of $(\Delta C_p - B_c)$ versus $|t|$ are given for fits 6 and 10 in Fig. 5. Since there are so many data points available, only every third point is shown in Fig. 5 for clarity. As can be seen from Figs. 4 and 5, the region where fit 10 with $\alpha_{\rm eff}^+ \neq \alpha_{\rm eff}^-$ is better than fit 6 is for data far in the high-temperature tail ($t > 8 \times 10^{-3}$), which makes fits with $\alpha_{\rm eff}^+ \neq \alpha_{\rm eff}^-$ of dubious significance.

Figure 6 shows ΔC_p data for run 2c over a narrow temperature range of 1.2 K near the Sm-A–Hex-B transition. The open symbols closest to T_c represent data not used in the fits. None of the filled points used in the fitting analysis were subject to any distortion due to finite $|T_{\rm ac}|$ amplitude effects since the maximum value of $|T_{\rm ac}|$ was 8 mK zero to peak far from T_c and less near T_c. The deviations of the observed C_p points from the fit curve close to T_c are typical of those seen when two-phase coexistence exists with some smearing of the latent heat over a narrow temperature interval.

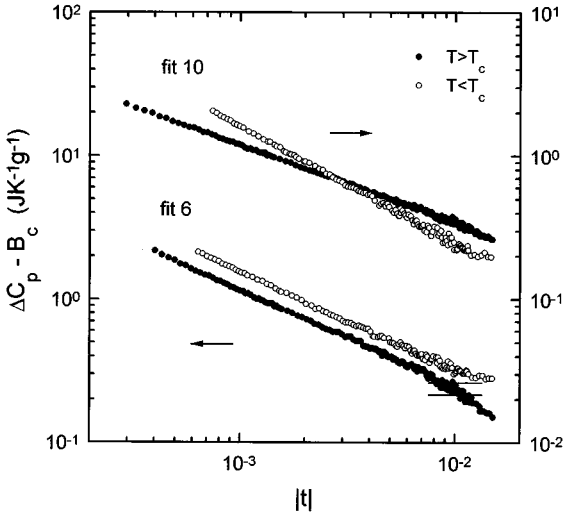

FIG. 5. Log-log plots of $(\Delta C_p - B_c)$ vs $|t|$ for 3(10)OBC run 2c data. The $B_c^\pm$ values are given in Table I for fits 6 and 10. A typical error bar is shown at $|t| = 10^{-2}$; the error bar is smaller than the size of the plotted points at $|t| \leqslant 10^{-3}$.

IV. DISCUSSION

The conclusion to be drawn from Table I, Figs. 4–6, and the above discussion of other fitting attempts is that the 3(10)OBC transition is clearly first order but can be modeled by a power law form with either $B_c^+ \neq B_c^-$ or $\alpha_{\rm eff}^+ \neq \alpha_{\rm eff}^-$, both of which are classic indications of first-order transitions. The effective exponent $\alpha_{\rm eff}$ (or $\overline{\alpha_{\rm eff}}$) for our sample ($\sim 0.68$) agrees quite well with $\alpha_{\rm eff} = 0.65 \pm 0.05$ obtained recently for 65OBC [18], and the $\Delta B_c = B_c^+ - B_c^-$ values are similar in both cases since the average ΔB_c for 65OBC fits was 0.187.

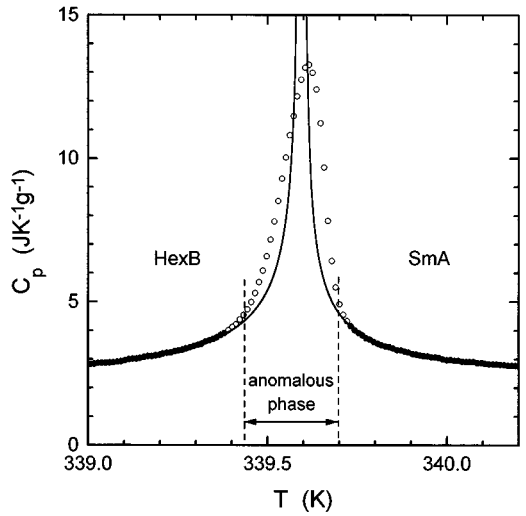

FIG. 6. C_p data close to the Sm-A–Hex-B transition temperature for 3(10)OBC run 2c. Open symbols (○) denote points not used in the fitting procedure. The ''theory curve'' represents fit 6. The vertical dashed lines mark the region of anomalous $[C_{\rm app} \sin\phi - (1/\omega R)]$ from Fig. 3.

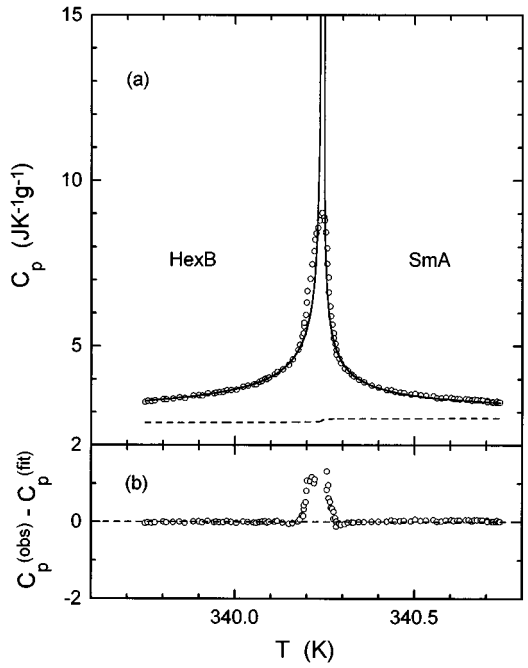

FIG. 7. (a) Plot of C_p data from Ref. [16] and the fitting curve $A^{\pm}|t|^{-\alpha_{\rm eff}}(1+D_1^{\pm}|t|^{0.75})+B$ given in that reference. The dashed curve represents $A^{\pm}D_1^{\pm}|t|^{0.75-\alpha_{\rm eff}}+B$ with $\alpha_{\rm eff}=0.59$ taken from [16]. Note that this empirical quantity exhibits a rounded step, thus acting much like $B_c^+ \neq B_c^-$ for our fits 4–7 with $D_1^{\pm}=0$. (b) Residuals $C_p(\text{obs})-C_p(\text{fit})$ for the above data. A gap of 60 mK was used in obtaining the fits reported in [16], but systematic deviations clearly extend over a $\sim$105 mK region.

We believe that the explicit breaking of scaling with $B_c^+ \neq B_c^-$ or $\alpha_{\rm eff}^+ \neq \alpha_{\rm eff}^-$ is expected since this transition is clearly first order. The use of the empirical $(1+D_1^{\pm}|t|^{0.75})$ correction form does not seem justified by theory or our fitting results; see also footnote 17 in Ref. [13].

Our exponent $\alpha_{\rm eff}=0.68\pm0.10$ differs considerably from the $\alpha_{\rm eff}$ values of 0.56 and 0.59 reported previously [13,15,16], and the magnitudes of ΔC_p differ considerably (see Fig. 2 and the text in Sec. II). Thus we give in Fig. 7 a plot of C_p data from Ref. [16] with the fitting curve reported there and the residuals from that fit. It is clear from this figure that there are systematic deviations of the data in Ref. [16] from the fit curve over a region of about 105 mK. Although the width of this first-order coexistence is smaller than in our sample, we believe that the behavior of both samples is qualitatively the same. As a demonstration of the rounded step nature of the $A^{\pm}D_1^{\pm}|t|^{0.75-\alpha_{\rm eff}}$ correction terms, we show as a dashed line in Fig. 7 the quantity $A^{\pm}D_1^{\pm}|t|^{0.75-\alpha_{\rm eff}}+B$, where $B=B_r+B_c$ is given in Ref. [16] and it is stated there that the regular contribution $E\Delta T$ to the slope of C_p(background) is zero. The difference between the quantity $[AD_1|t|^{0.75-\alpha_{\rm eff}}+B]$ at $t=+10^{-2}$ and $t=-10^{-2}$ is 0.189 J K^{-1} g^{-1}, and comparable pseudosteps occur in other nmOBC compounds [13]. The magnitude of this 3(10)OBC rounded step is comparable to our ΔB_c steps in fits 5–7.

A comparison of the *absolute* values reported for ''T_c'' may be of some value. Our value is 339.62 ± 0.15 K. The value given in Refs. [13] and [16] is 340.24 K; and that given in Ref. [15] is 340.37 K, which is a bit odd since the C_p data sets are the same in Refs. [13] and [15] but different in Refs. [13] and [16]. The absolute accuracy in these latter cases is not given, but can be estimated to be ±0.20 K [17]. Thus the samples studied in Refs. [13–16] may be of higher purity, but the sharp melting transition for our sample indicates that the present sample is quite good.

The Sm-A–Hex-B transition in all nmOBC compounds and binary mixtures that exhibit the Sm-A–Hex-B–Cr-E sequence and also 3(10)OBC, where the sequence is Sm-A–Hex-B–Cr-X, have been reported to be second order [1]. However, a recent calorimetric study of 65OBC provides evidence of an extremely weak first-order transition with dominant pretransitional wings [18], and the present study shows that 3(10)OBC is clearly a weak first-order transition. Indeed, we believe that all Sm-A–Hex-B transitions may be weakly first order, usually with small smeared latent heat effects which round the C_p peaks, as is usually the case in other nmOBC data with the possible exception of 37OBC [14].

It is proposed in Ref. [18] that Sm-A–Hex-B transitions are *quasitricritical* (or perhaps *quasitetracritical*) in the sense of Bergman and Halperin [26], who developed the theory of a compressible Ising model. In the present case, quasicritically could arise from a $|\Psi|^2\rho$ or $|\Psi|^2$ (strain) coupling between the amplitude of the XY hexatic order parameter Ψ and the in-plane positional density ρ or strain; see Ref. [18] for further details. Without such coupling, the latent heat ΔH along the first-order section of the phase transition line decreases to zero at an isolated tricritical point and remains zero along the subsequent second-order section of the transition line. A quasitricritical system is always first order, with ΔH decreasing rapidly to a small value but continuing to be nonzero along what would be the second-order section in the absence of coupling [26]. Such quasicriticality could explain a line of Sm-A–Hex-B transitions with anomalous $\alpha_{\rm eff}$ values. For 3(10) OBC, ΔH is small but the first-order character is easily detected. Thus it should lie near a triple point (Sm-A–Hex-B–Hex-I in this case), where conventional tricritical points are predicted [9,10], and this seems to be borne out by a generalized smectic-hexatic phase diagram [27] as well as data in Ref. [15]. On the other hand, 65OBC should lie considerably further from such a triple point since the first-order character is very weak, and this also seems to fit well with the generalized smectic-hexatic diagram.

It should be noted that there is some evidence that the Sm-A–Hex-B transition in bulk 65OBC exhibits Gaussian pseudocritical behavior [18], which is consistent with the idea of a quasicritical transition. If the theoretical fixed point that determines the quasicritical behavior prior to the first-order instability is tricritical the heat capacity exponent α associated with that point is $\alpha=1/2$, whereas a tetracritical fixed point has a characteristic α value of 2/3. The 3(10)OBC effective exponent $\alpha_{\rm eff}=0.68\pm0.10$ is very close to the tetracritical value, but that may be accidental since there is no clear reason for a dominant tetracritical point. If quasitricriticality is involved, the problem is to reconcile $\alpha_{\rm eff}=0.68$ with the expected α value of 0.5.

Additional experiments on bulk nmOBC compounds, especially high-resolution data concerning the in-plane posi-

tional order, are needed. Much interesting work has already been done on very thin film samples [1,28–30], but these have a distinctly different critical behavior from bulk samples and well may be second order. In any case, the behavior of two-layer films differs dramatically at the Sm-A–Hex-B transition from that expected from the 2D XY model.

ACKNOWLEDGMENTS

The authors wish to thank C. C. Huang for providing the 3(10)OBC sample, originally synthesized by J. W. Goodby, and both C. C. Huang and G. Iannacchione for many helpful discussions. This work was supported in part by the National Science Foundation under Grant No. DMR 93-11853.

[1] C. C. Huang and T. Stoebe, Adv. Phys. **42**, 343 (1993), and references cited therein.
[2] R. Pindak, D. E. Moncton, S. C. Davey, and J. W. Goodby, Phys. Rev. Lett. **46**, 1135 (1981); J. W. Goodby and R. Pindak, Mol. Cryst. Liq. Cryst. **75**, 233 (1981).
[3] S. C. Davey, J. Budai, R. Pindak, J. W. Goodby, and D. E. Moncton, Phys. Rev. Lett. **53**, 2129 (1984).
[4] J. D. Brock, A. Aharony, R. J. Birgeneau, K. W. Evans-Lutterodt, J. D. Litster, P. M. Horn, G. B. Stephenson, and A. R. Tajbakhsh, Phys. Rev. Lett. **57**, 98 (1986); J. D. Brock, D. Y. Noh, B. R. McClain, J. D. Litster, R. J. Birgeneau, A. Aharony, P. M. Horn, and J. C. Liang, Z. Phys. B **74**, 197 (1989); these results pertain to the *tilted* Sm-C–Sm-I supercritical evolution in 8OSI.
[5] E. Gorecka, L. Chen, S. Kumar, A. Krowczynski, and W. Pyzuk, Phys. Rev. E **50**, 2863 (1994).
[6] C.-F. Chou, J. T. Ho, S. W. Hui, and V. Surendranath, Phys. Rev. Lett. **76**, 4556 (1996), and references cited therein.
[7] R. Bruinsma and G. Aeppli, Phys. Rev. Lett. **48**, 1625 (1982).
[8] G. Aeppli and R. Bruinsma, Phys. Rev. Lett. **53**, 2133 (1984).
[9] A. Aharony, R. J. Birgeneau, J. D. Brock, and J. D. Litster, Phys. Rev. Lett. **57**, 1012 (1986).
[10] J. V. Selinger, J. Phys. (Paris) **49**, 1387 (1988).
[11] C. Rosenblatt and J. T. Ho, Phys. Rev. A **26**, 2293 (1982); see footnote 14 in this paper.
[12] E. Gorecka, L. Chen, A. Lavrentovich, and W. Pyzuk, Europhys. Lett. **27**, 507 (1994).
[13] G. Nounesis, R. Geer, H. Y. Liu, C. C. Huang, and J. W. Goodby, Phys. Rev. A **40**, 5468 (1989); see footnote 17 in this paper.
[14] T. Pitchford, G. Nounesis, D. Dumrongrattana, J. M. Viner, C. C. Huang, and J. W. Goodby, Phys. Rev. A **32**, 1938 (1985).
[15] T. Pitchford *et al.*, Phys. Rev. A **34**, 2422 (1986).
[16] C. C. Huang, G. Nounesis, R. Geer, J. W. Goodby, and D. Guillon, Phys. Rev. A **39**, 3741 (1989).
[17] C. C. Huang (private communication).
[18] H. Haga, Z. Kutnjak, G. Iannacchione, S. Qian, D. Finotello, and C. W. Garland, Phys. Rev. E **56**, 1808 (1997).
[19] T. Stoebe, J. T. Ho, and C. C. Huang, J. Thermophys. **15**, 1189 (1994).
[20] C. W. Garland, Thermochim. Acta **88**, 127 (1985); in Liquid Crystals: Physical Properties and Phase Transitions, edited by S. Kumar (Cambridge University Press, New York, in press), Chap. 6 and references cited therein.
[21] H. Yao, T. Chan, and C. W. Garland, Phys. Rev. E **51**, 4585 (1995); Z. Kutnjak, C. W. Garland, C. G. Schatz, P. J. Collings, C. J. Booth, and J. W. Goodby, *ibid.* **53**, 4955 (1996).
[22] H. Yao, K. Ema, and C. W. Garland, Rev. Sci. Instrum. (to be published).
[23] C. W. Garland, G. Nounesis, M. J. Young, and R. J. Birgeneau, Phys. Rev. E **47**, 1918 (1993).
[24] J. Thoen, in *Phase Transitions in Liquid Crystals*, edited by S. Martellucci (Plenum, New York, 1992). Chap. 10 and references cited therein.
[25] R. Mahmood, M. Lewis, D. Johnson, and V. Surendranath, Phys. Rev. A **38**, 4299 (1988).
[26] D. J. Bergman and B. I. Halperin, Phys. Rev. B **13**, 2145 (1976); see also M. A. deMoura, T. C. Lubensky, Y. Imry, and A. Aharoney, *ibid.* **13**, 2176 (1976).
[27] Z. Kutnjak and C. W. Garland (unpublished).
[28] T. Stoebe, C. C. Huang, and J. W. Goodby, Phys. Rev. Lett. **68**, 2944 (1992).
[29] C.-F. Chou, J. T. Ho, S. W. Hui, and V. Surendranath, Phys. Rev. Lett. **76**, 4556 (1996).
[30] A. J. Jin *et al.*, Phys. Rev. Lett. **74**, 4863 (1995); Phys. Rev. E **53**, 3639 (1996).